Effect of deformation parameters, Q value, and finite-range NN force on α-particle preformation probability

M. Ismail[1] and A. Adel[1,2,*]

[1]*Physics Department, Faculty of Science, Cairo University, Giza, Egypt*

[2]*Physics Department, College of Science, Majmaah University, Al-Zulfi, Kingdom of Saudi Arabia*

(Received 22 December 2013; revised manuscript received 26 February 2014; published 21 March 2014)

The influence of nuclear deformation on α-decay half-lives is taken into account in the deformed density-dependent cluster model. The microscopic potential between the spherical α particle and the deformed daughter nucleus is evaluated numerically from the double-folding model by the multipole expansion method. A realistic density-dependent nucleon-nucleon (NN) interaction with finite-range exchange part, which produces the nuclear matter saturation curve and the energy dependence of the nucleon-nucleus optical potential model is used. The ordinary zero-range exchange NN force, which is commonly used in α decay, is also considered in the present work. We systematically investigate the influence of nuclear deformations on the α-particle preformation probability of the deformed medium and heavy nuclei from the ground state to ground-state α transitions within the framework of the Wentzel-Kramers-Brillouin method by considering the Bohr-Sommerfeld quantization condition. Taking the deformation of daughter nuclei into account changes the behavior of the preformation probability, S_α, by an amount depending on the Q value, the order, values, and signs of deformation parameters. Calculations have been conducted for the spherical nuclei in order to present clearly the effect of the deformation on the preformation probability. The combined effect of both finite-range force and deformation can reduce the value of S_α by about an order of magnitude.

DOI: 10.1103/PhysRevC.89.034617 PACS number(s): 23.60.+e, 21.10.Jx, 21.10.Tg, 21.30.Fe

I. INTRODUCTION

α emission is one of the prominent decay channels of the heavy and superheavy nuclei (SHN) [1]. Measurements on the α decay can provide reliable information on the nuclear structure such as the ground-state half-life, the nuclear spin and parity, the shell effects, and the nuclear charge radii [2–8]. Studying the decay properties of superheavy elements, primarily by α emissions, has become an important domain of intense research [9–11]. α-decay chains are crucial in the identification and recognition of new superheavy elements or isotopes.

Extensive theoretical studies have been devoted to pursuing a quantitative description of α-decay half-lives by both phenomenological and microscopic methods. Different methods have been used to determine the α-decay half-lives both experimentally and theoretically. Different empirical formulas with adjustable parameters have been proposed, such as the Geiger and Nuttall [12], Viola-Seaborg [13], Parkhomenko-Sobiczewski [14], and Denisov formulas [15] to deduce experimental data. Such analytical expressions are very useful for experimentalists who need to evaluate the expected half lives during the design of experiments and to rapidly check the measured decay energies and half-lives after experiments, especially for newly synthesized superheavy nuclei.

Moreover, semimicroscopic and microscopic approaches have been widely applied to calculate α-decay half-lives such as the density dependent cluster model (DDCM) [16], the generalized liquid drop model (GLDM) [17], Coulomb, and proximity potential model [18,19].

Calculation of the penetration probability requires a reliable input of the α-nucleus interaction potential, which consists of both Coulomb repulsive and nuclear attractive parts. The Coulomb part is well known, but the nuclear part is less well defined. A double-folding model with a realistic M3Y NN interaction has been successfully used in the calculations of α-decay half-lives. For example, Basu [20] calculated the half-lives for α decay and cluster-radioactivity in the superasymmetric fission model with microscopic nuclear potential based on the double folding of the nuclear density distributions of the two composite nuclear fragments with the realistic M3Y effective interaction. Chowdhury *et al.* [21] have used the density-dependent M3Y (DDM3Y) effective nucleon-nucleon interaction in their calculations of α-decay half-lives. Xu and Ren [16] have presented a systematic calculation on α-decay half-lives in the framework of DDCM in which the nuclear potential is obtained from renormalized M3Y NN in the double-folding model. In most of the previous calculations of the α-particle decay processes, it is assumed that the exchange part of the NN interaction has a zero range. By this assumption, one neglects antisymmetrization between the nucleons in the α particle and the nucleons in the daughter nucleus, which is essential to satisfy the Pauli exclusion principle. The main features of the adopted version of the folding model are the inclusion of a realistic density dependence into the effective NN interaction and the explicit treatment of the exchange potential using a realistic local approximation.

Various calculations with different potentials are usually performed with the assumption of spherical shapes. As many ground-state α emitters are deformed, considering an angle-dependent potential looks quite logical. Although the spherical model has been successful to some extent, it is useful to work

*ahmedshosha200@yahoo.com

beyond the spherical approximation and to include new factors such as nuclear deformation and knock-on exchange effects.

Many theoretical models for α decay included the deformation effect on α-decay half-lives [6,19,22]. Rasmussen and Segall [23] have performed the first computations of the α-decay widths in rotational nuclei by using the coupled channels method. Santhosh and coworkers [24] have investigated the α decay of even-odd and odd-even nuclei [25] by using the Coulomb and proximity potential model for the deformed nuclei (CPPMDN) in the framework of WKB approximation. Xu and Ren [26] have performed a global calculation of favored α-decay half-lives of both even-A and odd-A deformed nuclei in the framework of a deformed version of the density-dependent cluster model (DDCM). Coban and coworkers [27] have investigated the influence of nuclear deformations on the α-decay half-lives within the framework of WKB approximation. Denisov and coworkers [28,29] have studied the α-decay half-lives and the α-capture cross sections in the framework of a unified model for the α decay and α capture (UMADAC) with deformed nuclear and Coulomb potential.

Deformation is reflected in orientation angle dependent nuclear radius [22], which leads to enhanced penetration for larger radii and reduced penetration for smaller radii. Owing to the exponential dependence of the calculated half-life on the penetration factor, the half-life is reduced for a deformed nucleus compared to the spherical one. Since the preformation probability could be calculated as the ratio between calculated and experimental half-life times, we expect that deformation reduces the value of preformation factor S_α. The reduction for a certain nucleus depends on the values and orders of deformation parameters present in the daughter nucleus. This leads to change in the behavior of S_α with N or Z numbers when deformation is switched on. These changes may produce a minimum, which is not present when spherical case is considered. It should be noted that the behavior of S_α with N or Z is used to determine magic and semimagic numbers especially for superheavy nuclei where most nuclear structure is still unknown. Also, the behavior of S_α has been correlated recently to the energy levels of the parent nucleus [5,30].

In the present work, our aim is to investigate the role of deformation and knock-on exchange effects in explaining the preformation probability and α-decay half-lives of the deformed nuclei. The α-decay half-lives have been determined using microscopic potentials within the semiclassical WKB approximation in combination with Bohr-Sommerfeld quantization condition. The microscopic α-nucleus potential is numerically constructed in the well-established double-folding model for both Coulomb and nuclear potentials. A realistic density-dependent M3Y interaction, based on the G-matrix elements of the Paris NN potential, has been used in the folding calculation. The main effect of antisymmetrization under exchange of nucleons between the α and daughter nuclei has been included in the folding model through the finite-range exchange part of the NN interaction. The local approximation for the nondiagonal one-body density matrix in the calculation of the exchange potential was included by using the harmonic oscillator representation of the nondiagonal density matrix of the α particle [31,32]. The preformation factor, S_α, is extracted from the experimental α-decay half-life.

This paper is organized as follows. In Sec. II the double-folding model is introduced and the methods for determining the decay width, penetration probability, assault frequency, and preformation probability are presented. In Sec. III the calculated results are presented and discussed. The conclusion is given in Sec. IV.

II. THEORETICAL FRAMEWORK

Based on the assumption that an α particle interacts with an axially symmetric deformed core nucleus, the total interaction potential of the α-core system, comprising the nuclear and Coulomb potentials plus the centrifugal part, is given as [4,16]

$$V_{\mathrm{T}}(R,\theta) = \lambda(\theta)\, V_N(R,\theta) + V_C(R,\theta) + \frac{\hbar^2}{2\,\mu}\frac{\left(\ell+\frac{1}{2}\right)^2}{R^2}, \quad (1)$$

where the renormalization factor $\lambda(\theta)$ is the depth of the nuclear potential, R is the separation between the mass center of α particle and the mass center of core, θ is the orientation angle of the deformed nucleus, as shown in Fig. 1, and ℓ is the angular momentum carried by the α particle.

The total nuclear interaction $V_N(R,\theta)$ is the sum of direct, $V_d(R,\theta)$, and exchange, $V_{Ex}(R,\theta)$, parts. They are given by [32,33]

$$V_D(R,\theta) = \int d\vec{r}_1 \int d\vec{r}_2 \rho_\alpha(\vec{r}_1)\, \upsilon_D(\rho,s)\, \rho_d(\vec{r}_2), \quad (2)$$

$$V_{Ex}(R,\theta) = \int d\vec{r}_1 \int d\vec{r}_2 \rho_\alpha(\vec{r}_1,\vec{r}_1+\vec{s})\, \rho_d(\vec{r}_2,\vec{r}_2-\vec{s}) \times \upsilon_{Ex}(\rho,s) \exp\left[\frac{i\vec{k}(R,\theta)\cdot\vec{s}}{M}\right], \quad (3)$$

where $\vec{s} = \vec{r}_2 - \vec{r}_1 + \vec{R}$ is the relative distance between a constituent nucleon in the α particle and one in the core nucleus and υ_D is the nucleon-nucleon NN interaction. $\rho_\alpha(\vec{r}_1)$ and $\rho_d(\vec{r}_2)$ are, respectively, the matter density distributions of the α particle and residual core nucleus.

The method of calculating the $V_D(R,\theta)$ and $V_C(R,\theta)$ is outlined in Refs. [34,35] based on the multipole expansion of the deformed nucleus density distribution then using the Fourier transform of the finite-range NN interaction to separate the coupled coordinates.

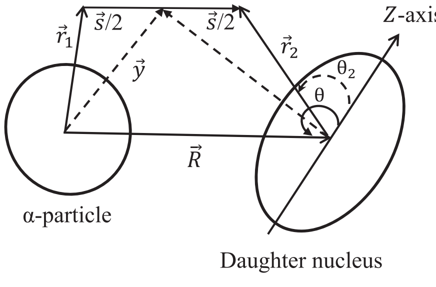

FIG. 1. Schematic representation of two interacting spherical and axially symmetric deformed nuclei. The orientation angle of the deformed nucleus is θ.

The matter density distribution of the α particle is a standard Gaussian form, namely

$$\rho_\alpha(r_1) = 0.4229 \exp\left(-0.7024\, r_1^2\right). \tag{4}$$

The density distribution of the daughter nucleus is supposed to be in a deformed Fermi form given by

$$\rho_d(r_2,\theta_2) = \frac{\rho_0}{1+\exp\left(\frac{r_2 - R(\theta_2)}{a}\right)}, \tag{5}$$

where θ_2 is the angle between $\vec{r}_2$ and the symmetry axis of the deformed daughter nucleus. The value of ρ_0 is determined by integrating the density distribution equivalent to the mass number or atomic number of the corresponding daughter nucleus for the nuclear and Coulomb potentials, respectively. The nuclear radius parameter $R(\theta_2)$ parameterized in the usual way,

$$R(\theta_2) = R_0[1 + \beta_2 Y_{2,0}(\theta_2) + \beta_4 Y_{4,0}(\theta_2)]. \tag{6}$$

The quadrupole and hexadecapole deformation parameters of the residual daughter nucleus, i.e., β_2 and β_4, are chosen as the evaluated values obtained by Moller *et al.* [36]. The half-density radius, R_0, and the diffuseness parameter, a, are given by [4,16]

$$R_0 = 1.07 A_d^{1/3}\ \text{fm}, \quad a = 0.54\ \text{fm}. \tag{7}$$

The local momentum of relative motion $k(R,\theta)$ is determined as

$$k^2(R,\theta) = \frac{2\mu}{\hbar^2}\left[E_{\text{c.m.}} - V_N(R,\theta) - V_C(R,\theta)\right], \tag{8}$$

where μ is the reduced mass for the reacting nuclei, $E_{\text{c.m.}}$ is the center-of-mass (c.m.) energy. $V_N(R,\theta) = V_D(R,\theta) + V_{Ex}(R,\theta)$, and $V_C(R,\theta)$ are the total nuclear and Coulomb potentials, respectively.

The nonlocal densities of the interacting nuclei are approximated as [32]

$$\rho(\vec{r},\vec{r}+\vec{s}) \simeq \rho\left(\vec{r}+\frac{\vec{s}}{2}\right) \hat{j}_1\left[k_{\text{eff}}\left(\vec{r}+\frac{\vec{s}}{2}\right)s\right], \tag{9}$$

with

$$\hat{j}_1(x) = 3\, j_1(x)/x = 3(\sin x - x\cos x)/x^3. \tag{10}$$

The α particle is a unique case where a simple Gaussian can reproduce very well its ground-state density [33]. Assuming four nucleons to occupy the lowest $s\frac{1}{2}$ harmonic oscillator (h.o.) shell in ^{4}He, one obtains exactly the nondiagonal ground-state DM for the α particle as [31,32]

$$\rho_\alpha(\vec{r},\vec{r}+\vec{s}) \simeq \rho_\alpha\left(\left|\vec{r}+\frac{\vec{s}}{2}\right|\right) \exp\left(-\frac{s^2}{4\,b_\alpha^2}\right). \tag{11}$$

The local Fermi momentum $k_{\text{eff}}(r)$ is given by [32,37]

$$k_{\text{eff}}(\vec{r}) = \left\{\frac{5}{3\rho(\vec{r})}\left[\tau(\vec{r}) - \frac{1}{4}\nabla^2\rho(\vec{r})\right]\right\}^{1/2}. \tag{12}$$

Using the extended Thomas-Fermi approximation, the kinetic energy density is then given by

$$\tau(\vec{r}) = \frac{3}{5}\left(\frac{3\pi^2}{2}\right)^{2/3}\rho(\vec{r})^{5/3} + \frac{1}{3}\nabla^2\rho(\vec{r}) + \frac{1}{36}\frac{|\vec{\nabla}\rho(\vec{r})|^2}{\rho(\vec{r})}. \tag{13}$$

The first term in this expression stands for Thomas-Fermi approximation while the other two terms represent the surface correction.

One easily obtains the self-consistent and local exchange potential V_{Ex} as

$$\begin{aligned} V_{Ex}(R,\theta) = 4\pi c g(E) \int_0^\infty & ds\, s^2\, \upsilon_{Ex}(s)\, j_0(k(R,\theta)s/M) \\ &\times \int d\vec{y}\, \rho_d(\vec{y}-\vec{R})\, \hat{j}_1\left(k_{\text{eff}}^d(\vec{y}-\vec{R})s\right) \\ &\times \rho_\alpha(y) \exp\left(-\frac{s^2}{4\,b_\alpha^2}\right) \\ &\times \{1 + \alpha\exp[-\beta(\rho_\alpha(y) + \rho_d(\vec{y}-\vec{R}))] \\ &- \gamma[\rho_\alpha(y) + \rho_d(\vec{y}-\vec{R})]\}. \end{aligned} \tag{14}$$

V_{Ex} depends on the total potential, $V(R) = V_D + V_{Ex} + V_C$ through the relative motion momentum given by Eq. (8). So, the problem of obtaining $V(R)$ is a self-consistent problem. The exchange potential, Eq. (14), can then be evaluated by an iterative procedure which converges very fast.

We use a realistic NN interaction whose parameters reproduce consistently the equilibrium density, and binding energy of normal nuclear matter as well as the density and energy dependence of nuclear optical potential. The density-dependent M3Y-Paris effective NN force considered in the present work, CDM3Y1, has the factorized form [38],

$$\upsilon_D(\rho,s) = \left[11\,061.625\,\frac{e^{-4s}}{4\,s} - 2537.5\,\frac{e^{-2.5s}}{2.5\,s}\right] F(\rho)\, g(E), \tag{15}$$

$$\begin{aligned} \upsilon_{Ex}(\rho,s) = \Bigg[&-1524.25\,\frac{e^{-4s}}{4\,s} - 518.75\,\frac{e^{-2.5s}}{2.5\,s} \\ &- 7.8474\,\frac{e^{-0.7072s}}{0.7072\,s}\Bigg] F(\rho)\, g(E), \end{aligned} \tag{16}$$

with the density and energy dependence, respectively,

$$F(\rho) = c[1 + \alpha\exp(-\beta\rho) - \gamma\rho], \tag{17}$$

$$g(E) = (1 - 0.003 E_{Ap}). \tag{18}$$

The parameters c,α,β, and γ are adjusted to reproduce normal nuclear matter saturation properties for a given equation of state for cold nuclear matter. For CDM3Y1, $c = 0.3429$, $\alpha = 3.0232$, $\beta = 3.5512$ fm^3, and $\gamma = 0.5$ fm^3, which generate nuclear matter equation of state with incompressibility value, $K = 188$ MeV. E_{Ap} is the incident energy per projectile nucleon in the laboratory system.

In the case of a zero-range exchange NN interaction, $\upsilon_{Ex}(s)$ is expressed in terms of δ function as,

$$\upsilon_{Ex}(\vec{s}) = -590(1 - 0.002 E_{Ap})\,\delta(\vec{s}). \tag{19}$$

The renormalization factor $\lambda(\theta)$, introduced to the nuclear part of the folding potential is determined separately for each emission angle of α particle by applying the Bohr-Sommerfeld quantization condition [39],

$$\int_{R_1(\theta)}^{R_2(\theta)} dr \sqrt{\frac{2\mu}{\hbar^2}\,|V_T(r,\theta) - Q_\alpha|} = (G - \ell + 1)\,\frac{\pi}{2}, \tag{20}$$

where the global quantum number $G = 20\,(N > 126)$ and $G = 18\,(82 < N \leqslant 126)$ [16]. Q_α is the Q value of the α decay. $R_i(i = 1,2,3)$ are the three turning points for the α-daughter potential barrier where $V_T(r,\theta)|_{r=R_i} = Q_\alpha$.

It should be noted that the Bohr-Sommerfeld quantization, Eq. (20), is a requisite for the correct use of the WKB approximation. In Ref. [40], the half-lives are found to be sensitive to the implementation of this condition in the WKB approach, which fixes the depth of the double-folding nuclear potential λ. The application of this condition is correct for the case of spherical daughter nucleus because the periodicity of α-particle motion fulfills. In the present work, we have assumed a spherical α particle interacts with an axially symmetric deformed daughter nucleus and each decay through emission angle θ is a separate event. In this regard, the depth $\lambda(\theta)$ of the double-folding nuclear potential is determined separately for each emission angle of the α particle to ensure the quasibound Bohr-Sommerfeld condition. The same assumption, for deformed daughter nuclei, has been used by Coban *et al.* [27] for the calculation of α-decay half-lives and by Soylu *et al.* [41] in the calculation of cluster decay half-lives. In the deformed version of the density-dependent cluster model (DDCM), Xu and Ren [42] have also applied the Bohr-Sommerfeld condition to determine the depth of the double-folding potential separately for each decay.

The α-decay width Γ is given by [4,22,26]

$$\Gamma = \frac{\hbar}{4\mu}\, S_\alpha F\, P_\alpha, \tag{21}$$

where S_α is the spectroscopic factor (α-particle preformation probability), F and P_α are the average values of the normalization factor and the penetration probability, respectively:

$$F = \frac{1}{2}\int_0^\pi \frac{\sin\theta\, d\theta}{0.5 \times \int_{R_1(\theta)}^{R_2(\theta)} \frac{dr}{\sqrt{\frac{2\mu}{\hbar^2}|V_T(r,\theta)-Q_\alpha|}}} \tag{22}$$

$$P_\alpha = \frac{1}{2}\int_0^\pi \exp\left(-2\int_{R_2(\theta)}^{R_3(\theta)} dr\,\sqrt{\frac{2\,\mu}{\hbar^2}\,|V_T(r,\theta) - Q_\alpha|}\right) \times \sin\theta\, d\theta. \tag{23}$$

The α-decay half-life is related to the decay width, Γ, by the well-known expression [4,16,26]

$$T_{1/2} = \frac{\hbar \ln 2}{\Gamma}. \tag{24}$$

Finally, the spectroscopic factor (the preformation probability) of the α cluster inside the parent nucleus can be then obtained as the ratio of the calculated half-life, without S_α, to the experimental one [5,8,43],

$$S_\alpha = T_{1/2}^{\mathrm{cal}}/T_{1/2}^{\mathrm{exp}}. \tag{25}$$

III. RESULTS AND DISCUSSION

In Fig. 2, we illustrate the sum of the double-folding nuclear and Coulomb potentials for the interaction between the deformed daughter ^{234}Th nucleus and α particle in the decay of ^{238}U for two orientation angles $\theta = 0^o$ and $\theta = 90^o$ using finite-range (FR) or zero-range (ZR) exchange forces. The deformation of the daughter nucleus ^{234}Th is taken from Moller *et al.* [36]. If the deformation parameter equals zero, the double-folding α-core potential is automatically back to that of the spherical case. For deformed nuclei, the double-folding potentials are dependent on both the separation R and the orientation angle θ. For specific values of R, the total potential at $\theta = 0^\circ$ is more attractive in the medium region than that at $\theta = 90^\circ$. This is because there is a large overlap of nuclear density distribution at orientation angle $\theta = 0^\circ$.

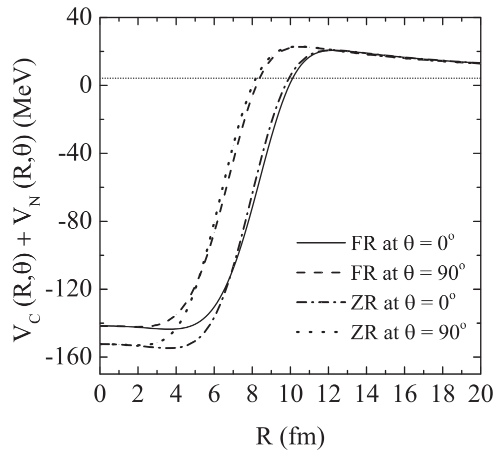

FIG. 2. Sum of double-folding nuclear and Coulomb potentials for the interaction between the deformed daughter ^{234}Th nucleus and α particle in the decay of ^{238}U for two orientation angles $\theta = 0^\circ$ and $\theta = 90^\circ$ using finite-range (FR) or zero-range (ZR) exchange forces.

Figure 3 shows the variation of the preformation probability with the neutron number for nine isotopes of Th nucleus. Figures 3(a) and 3(b) present respectively the calculations assuming deformed and spherical daughter nuclei. In each figure, we displayed the results of calculations using zero- and finite-range exchange *NN* interactions. The figures show that the realistic CDM3Y1-Paris *NN* interaction with finite-range exchange part affects the magnitude of the preformation factor without changing its behavior with neutron number variation; it reduces the value of S_α by a factor of about two and the behavior remains almost the same as for zero-range exchange *NN* interaction. Taking the deformation of daughter nuclei into account changes the behavior of S_α by an amount depending on the order, values, and signs of deformation parameters. For Th isotopes, hexadecapole deformation is almost absent except for ^{224}Th ($\beta_2 = 0.072$) and ^{226}Th ($\beta_2 = 0.092$), as shown on Table I. These two isotopes are prolate with β_2 values 0.103 and 0.130, respectively. The presence of the above-mentioned deformation parameters reduced the values of S_α for ^{224}Th and ^{226}Th by factors 0.77 and 0.62, respectively compared to the spherical case. The lightest two isotopes in Fig. 3 are oblate with β_2 values -0.13 and -0.104, respectively. Moreover, they have almost the same Q value. Negative values of deformation parameters besides absence of β_4 has very small effect on S_α, so the behavior of S_α is almost the same

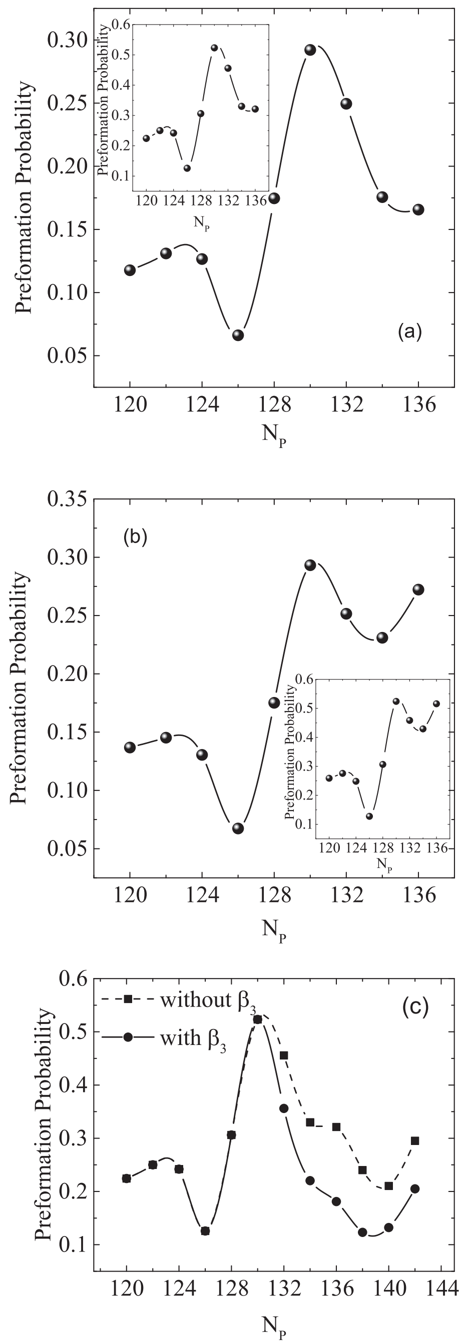

FIG. 3. Extracted α-preformation probability, S_α assuming (a) deformed daughter nuclei (b) spherical daughter nuclei using CDM3Y1-Paris NN interactions with finite-range exchange force, for different isotopes of Th nucleus with the parent neutron number, N_P. The insets are the corresponding calculations using zero-range exchange force. (c) shows the behavior of S_α with and without octupole deformation (β_3), the curves were calculated using zero-range exchange NN interaction.

for spherical and deformed isotopes in the neutron variation range $120 \leqslant N \leqslant 132$.

Some Th isotopes with neutron numbers in the range $132 \leqslant N \leqslant 142$ have octupole deformation parameter with negative values as indicated in Ref. [36]. We have used the ground-state octupole deformation β_3 corresponding to a specific shape in the Nilsson perturbed-spheroid parametrization (ϵ) of the recent data of Ref. [44]. The largest negative value of β_3 in this neutron range is $\beta_3 = -0.145$ at $N = 136$. Figure 3(c) shows the behavior of S_α with and without octupole deformation, the curves were calculated using zero-range exchange NN interaction. Figure 3(c) shows that when octupole deformation is switched on, it reduces the value of S_α by an amount depends on its value.

Figure 4 is the same as Fig. 3 but for U isotopes. Using the finite-range instead of the zero-range exchange NN force does not affect the behavior of S_α with neutron number variation but reduces its value by a factor of about 2. Table I shows that U isotopes differ in their Q values and deformation parameters compared to Th isotopes (all the isotopes are prolate). Figure 4 indicates that the behavior of the preformation probability with N variation is affected by deformation of the daughter nucleus and the Q-value variation of isotopes. For example, a minimum appears at $N = 136$, which shows that this number is a semimagic number, this is not clear when the deformation is absent. The minimum in S_α curve at $N = 142$ appears for both spherical and deformed daughters. Thus, the possibility that a minimum value of S_α appears when the deformation is taken into account exists. Minimum value in S_α at N value indicates some kind of stability or semimagic neutron number at this N value. This shows the importance of including the deformation in α-decay calculations. Figure 4(c) shows that the addition of the octupole deformation parameter to the calculations does not change the behavior of S_α with N variation. This is because the small values of β_3 possessed by U isotopes. The large variation of Q value for these isotopes produces deformation reduction factors in S_α ranging from 1.4 for ^{226}U to 4.2 for ^{238}U, the Q values of these two isotopes are 7.7 and 4.3 MeV, respectively. To show the effect of Q value in enhancing the deformation reduction factor of S_α, we present in Fig. 5 the β_2 variation of the deformation reduction factor F (defined as the ratio of S_α for spherical case to its value when deformation is added) at two values of hexadecapole deformation parameters ($\beta_4 = 0$ and 0.1). This figure contains the results for two U isotopes ^{222}U and ^{238}U, their Q values are 9.5 MeV and 4.3 MeV, respectively. The Figure shows that the value of the deformation reduction factor is less than 1.5 for small β_2 values ($\beta_2 < 0.1$), its value is affected strongly by the value of Q and increases to about 6 for $Q = 4.3$ MeV at $\beta_2 = 0.25$ and $\beta_4 = 0.1$. This value is reduced to less than 2.5 for the smaller Q value and less than 2 for the larger one when the hexadecapole deformation is switched off. This means that the value of Q plays important role in determining the value of the deformation reduction factor. For specific values of deformation parameters, small Q values is below the top barrier by large amount and the α particle goes long distance till it becomes free. In this case, it does not feel deformation compared to the case when the Q value is just below the barrier top. This is clear on Fig. 2 where the difference between the two orientations $\theta = 0^\circ$ and 90° becomes too small compared to the barrier width when we go down on the vertical axis. It should be noted that deformation affects only the value of the second turning point $R_2(\theta)$ [effect on $R_3(\theta)$ is too small].

TABLE I. The preformation probability S_α and the α-decay half-lives $T_{1/2}^{\rm calc}$ calculated without S_α for Th, U, Pu, and Cm isotopes using CDM3Y1 *NN* interactions. The experimental Q values and α-decay half-lives for the ground-state-to-ground-state transitions are taken from data compilations in Refs. [28,45].

Reaction	$Q_\alpha^{\rm exp}$ (MeV)	$T_{1/2}^{\rm exp}$ (s)	β_2^d	β_4^d	$S_\alpha^{\text{Sph-ZR}}$	$S_\alpha^{\text{Sph-FR}}$	$S_\alpha^{\text{Def-ZR}}$	$S_\alpha^{\text{Def-FR}}$
^{210}Th $\rightarrow {}^{206}$Ra + α	8.0690	1.62×10^{-2}	−0.130	−0.002	0.259	0.137	0.224	0.118
^{212}Th $\rightarrow {}^{208}$Ra + α	7.9580	3.17×10^{-2}	−0.104	0.004	0.276	0.145	0.250	0.131
^{214}Th $\rightarrow {}^{210}$Ra + α	7.8270	8.70×10^{-2}	−0.053	−0.007	0.249	0.130	0.242	0.127
^{216}Th $\rightarrow {}^{212}$Ra + α	8.0730	2.61×10^{-2}	−0.035	−0.015	0.128	0.067	0.126	0.066
^{218}Th $\rightarrow {}^{214}$Ra + α	9.8490	1.17×10^{-7}	0.008	0.008	0.307	0.175	0.306	0.175
^{220}Th $\rightarrow {}^{216}$Ra + α	8.9530	9.70×10^{-6}	0.008	0.008	0.524	0.293	0.523	0.292
^{222}Th $\rightarrow {}^{218}$Ra + α	8.1270	2.29×10^{-3}	0.020	0.010	0.458	0.252	0.456	0.250
^{224}Th $\rightarrow {}^{220}$Ra + α	7.2980	1.33×10^{0}	0.103	0.072	0.429	0.231	0.330	0.176
^{226}Th $\rightarrow {}^{222}$Ra + α	6.4509	2.43×10^{3}	0.130	0.092	0.516	0.272	0.321	0.166
^{222}U $\rightarrow {}^{218}$Th + α	9.5000	1.00×10^{-6}	0.008	0.008	1.047	0.585	1.045	0.582
^{224}U $\rightarrow {}^{220}$Th + α	8.6200	9.00×10^{-4}	0.030	0.019	0.232	0.127	0.229	0.125
^{226}U $\rightarrow {}^{222}$Th + α	7.7010	4.12×10^{-1}	0.111	0.081	0.355	0.190	0.254	0.134
^{228}U $\rightarrow {}^{224}$Th + α	6.8040	8.03×10^{2}	0.164	0.112	0.406	0.213	0.180	0.091
^{230}U $\rightarrow {}^{226}$Th + α	5.9927	2.67×10^{6}	0.173	0.111	0.601	0.310	0.232	0.115
^{232}U $\rightarrow {}^{228}$Th + α	5.4136	3.19×10^{9}	0.182	0.112	0.684	0.348	0.247	0.120
^{234}U $\rightarrow {}^{230}$Th + α	4.8598	1.09×10^{13}	0.198	0.115	0.439	0.220	0.132	0.063
^{236}U $\rightarrow {}^{232}$Th + α	4.5701	9.99×10^{14}	0.207	0.108	0.706	0.352	0.232	0.109
^{238}U $\rightarrow {}^{234}$Th + α	4.2700	1.78×10^{17}	0.215	0.102	1.432	0.709	0.339	0.159
^{228}Pu $\rightarrow {}^{224}$U + α	7.9400	1.10×10^{0}	0.146	0.100	0.133	0.071	0.073	0.038
^{230}Pu $\rightarrow {}^{226}$U + α	7.1800	1.02×10^{2}	0.172	0.111	0.753	0.393	0.313	0.157
^{232}Pu $\rightarrow {}^{228}$U + α	6.7160	1.36×10^{4}	0.191	0.114	0.405	0.209	0.147	0.073
^{234}Pu $\rightarrow {}^{230}$U + α	6.3100	7.73×10^{5}	0.199	0.115	0.508	0.260	0.155	0.076
^{236}Pu $\rightarrow {}^{232}$U + α	5.8671	1.31×10^{8}	0.207	0.117	0.413	0.209	0.123	0.059
^{238}Pu $\rightarrow {}^{234}$U + α	5.5932	3.90×10^{9}	0.215	0.110	0.483	0.243	0.139	0.067
^{240}Pu $\rightarrow {}^{236}$U + α	5.2558	2.84×10^{11}	0.215	0.102	0.753	0.375	0.190	0.090
^{242}Pu $\rightarrow {}^{238}$U + α	4.9845	1.54×10^{13}	0.215	0.093	0.491	0.243	0.146	0.069
^{244}Pu $\rightarrow {}^{240}$U + α	4.6655	3.18×10^{15}	0.224	0.079	0.443	0.218	0.152	0.071
^{238}Cm $\rightarrow {}^{234}$Pu + α	6.6700	3.24×10^{5}	0.216	0.109	0.205	0.104	0.060	0.029
^{240}Cm $\rightarrow {}^{236}$Pu + α	6.3978	3.29×10^{6}	0.215	0.11	0.360	0.182	0.096	0.046
^{242}Cm $\rightarrow {}^{238}$Pu + α	6.2156	1.90×10^{7}	0.215	0.102	0.418	0.210	0.118	0.057
^{244}Cm $\rightarrow {}^{240}$Pu + α	5.9017	7.43×10^{8}	0.223	0.087	0.364	0.182	0.122	0.058
^{246}Cm $\rightarrow {}^{242}$Pu + α	5.4751	1.83×10^{11}	0.224	0.071	0.540	0.267	0.164	0.077
^{248}Cm $\rightarrow {}^{244}$Pu + α	5.1617	1.46×10^{13}	0.224	0.062	0.444	0.218	0.145	0.068
^{246}Fm $\rightarrow {}^{242}$Cf + α	8.3770	1.49×10^{0}	0.224	0.079	0.546	–	0.197	–
^{248}Fm $\rightarrow {}^{244}$Cf + α	7.9940	4.86×10^{1}	0.234	0.073	0.317	–	0.109	–
^{250}Fm $\rightarrow {}^{246}$Cf + α	7.5570	2.40×10^{3}	0.234	0.057	0.247	–	0.089	–
^{252}Fm $\rightarrow {}^{248}$Cf + α	7.1527	1.09×10^{5}	0.235	0.040	0.209	–	0.085	–
^{254}Fm $\rightarrow {}^{250}$Cf + α	7.3075	1.37×10^{4}	0.245	0.026	0.356	–	0.144	–
^{256}Fm $\rightarrow {}^{252}$Cf + α	7.0270	1.37×10^{5}	0.236	0.015	0.509	–	0.230	–

Figure 6 presents our results for Pu isotopes. This figure shows small changes in the behavior between curves calculated with and without deformation parameters. The reason for this is that the isotopes on this figure have small changes in the values of β_2 and β_4 deformation parameters and their Q values differ from 7.9 MeV to 4.7 MeV as shown on Table I. If two adjacent isotopes have the same values of deformation parameters and nearly equal Q values, S_α for them are reduced by almost the same amount compared to the case when the deformation is absent. For example, the deformation parameters for the five isotopes of $^{232-240}$Pu vary by 11% for β_2 and 13% for β_4 and their Q values decrease by 21%, this variation in the values of parameters and Q values is reflected in almost similar behavior of S_α for both spherical and deformed cases for these isotopes. The deformation reduction factor of S_α increases from 2.8 for ^{232}Pu to 4.0 for ^{240}Pu.

Figure 7 is the same as Fig. 6 but for Cm isotopes. Table I indicates almost constant β_2 values for Cm isotopes while β_4 and the Q values decrease. The deformation reduction factor, in this case, is a competition between β_4 and Q value, the increase in β_4 value and the decrease in Q value both increase the deformation factor. For ^{238}Cm and ^{240}Cm, the deformation reduction factors are 3.4 and 3.8, respectively. Since β_4 has the same value for the two isotopes, the increase is due to lowering the Q value by 0.27 MeV. For ^{242}Cm, the value of the deformation reduction factor decreases to 3.5 due to the

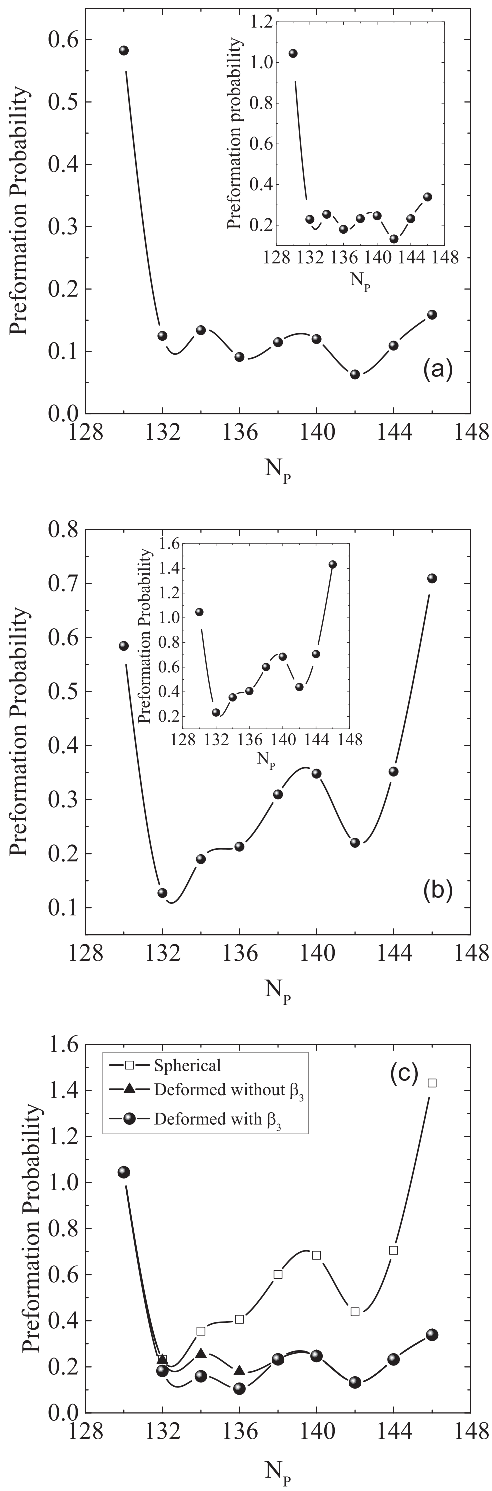

FIG. 4. The same as Fig. 3 but for U isotopes.

variation of Q value by 0.18 MeV and decrease in β_4 value by about 7%. It becomes 3.0 for ^{244}Cm due to the large reduction in β_4 value by about 15% compared to the isotope ^{242}Cm, although Q value decreased by 0.3 MeV. This small reduction produces a minimum in the spherical case, at $N = 148$.

Figure 8 shows the results for the element Fm using zero-range exchange NN interaction with and without deformation.

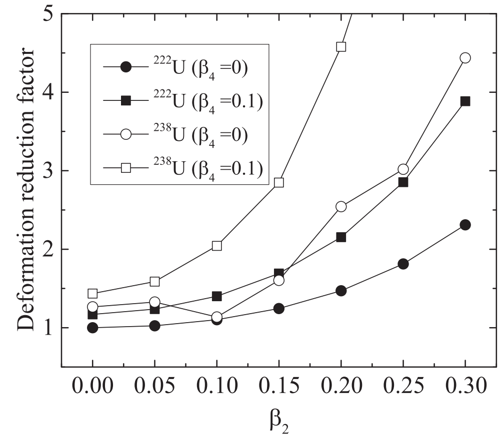

FIG. 5. The β_2 variation of the deformation reduction factor F (defined as the ratio of S_α for spherical case to its value when deformation is added) at two hexadecapole deformation parameters ($\beta_4 = 0, 0.1$) for two U isotopes ^{222}U and ^{238}U isotopes.

Again β_2 have almost constant values but β_4 varies in a wide range of values (0.015–0.079). The variation of the deformation reduction factor is governed by variations in β_4 and Q values. Its smallest value is 2.2 for the ^{256}Fm isotope

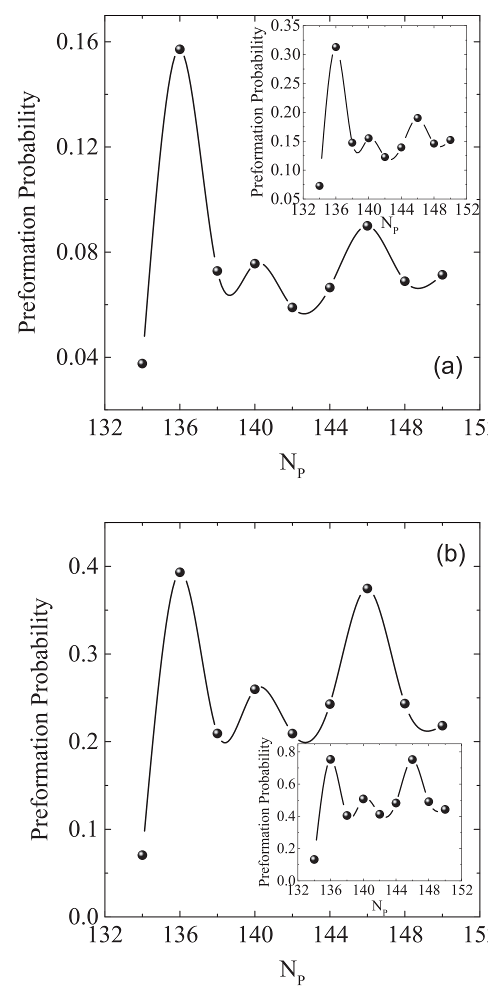

FIG. 6. The same as Fig. 3 but for Pu isotopes.

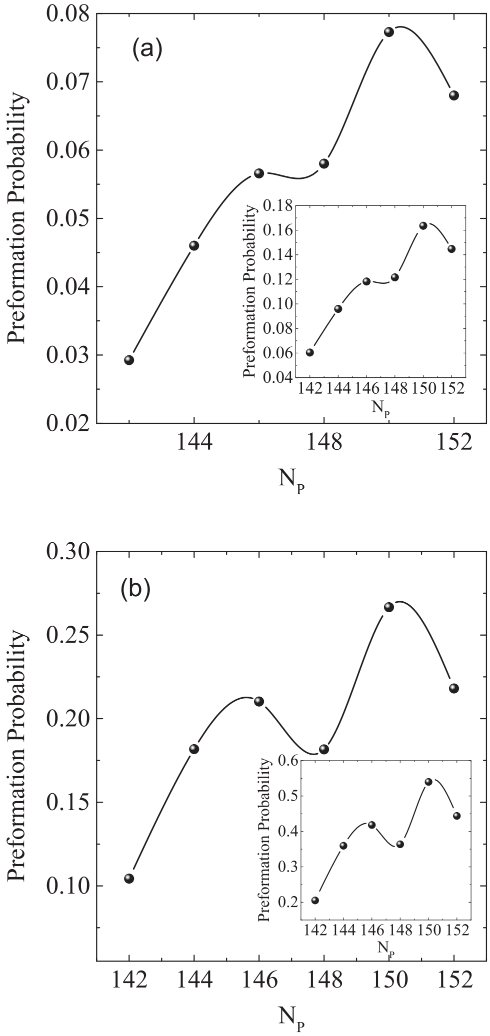

FIG. 7. The same as Fig. 3 but for Cm isotopes.

whose Q value and β_4 value are the lowest ($Q = 7.03$ MeV, $\beta_4 = 0.015$). The largest value of deformation reduction factor is 2.9 for ^{248}Fm where $\beta_4 = 0.073$ and $Q = 8$ MeV. The next point for ^{250}Fm is reduced also by almost the same factor

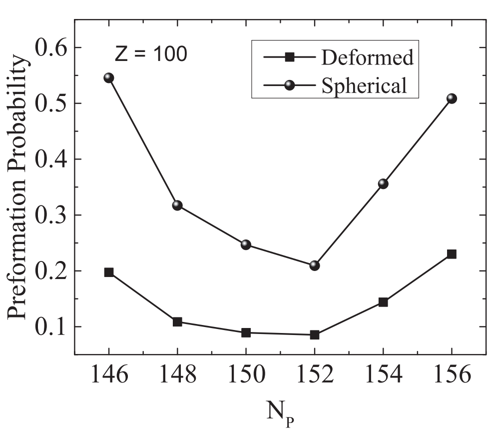

FIG. 8. Extracted α-preformation probability, S_α using CDM3Y1-Paris *NN* interactions with zero-range exchange force, for different isotopes of Fm nucleus with and without deformation.

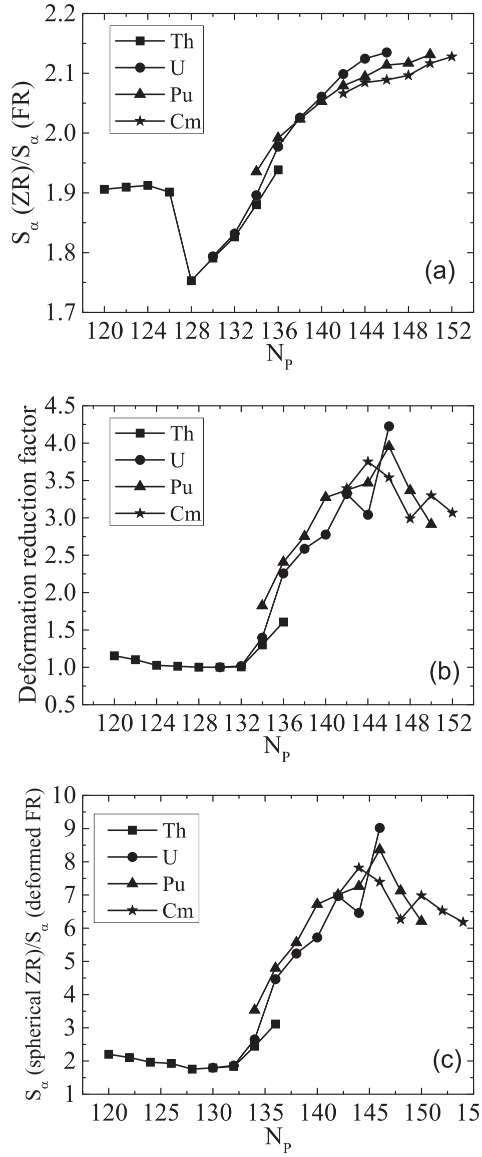

FIG. 9. (a) shows the neutron number variation of the ratio of preformation probabilities calculated using zero-range and finite-range *NN* force for the different isotopes of the nuclei Th, U, Pu, and Cm. (b) is the same as (a) except that it is for the deformation reduction factor F. (c) shows the neutron number variation of the ratio of S_α calculated assuming spherical nucleus and zero-range *NN* force and S_α for deformed nucleus derived from finite-range *NN* force.

($F = 2.8$) since the decrease of both β_4 and Q value produced the same F value. For ^{252}Fm, the Q value decreased by the same amount as ^{250}Fm and β_4 decreased by 30%, this large decrease in β_4 lowered the F value to 2.5. For ^{254}Fm, the small increase in β_2 and the increase in Q value by about 0.16 MeV overcome the large decrease in β_4 (35%) resulting in the same F value. This change in F values produced more shallow minimum at $N = 152$ compared to the spherical case.

Figure 9(a) shows the neutron number variation of the ratio of preformation probabilities calculated using zero-range and finite-range *NN* force for the different isotopes of the nuclei Th, U, Pu, and Cm. The calculations, in Fig. 9(a), are performed assuming deformed daughter nuclei. The figure shows that finite-range exchange *NN* force (realistic CDM3Y1 *NN* interaction) reduces the value of S_α by a factor ranging between 1.75 and 2.15. The figure shows a clear minimum at the neutron number $N = 128$, this indicates that the finite-range force has a small effect on the value of S_α when the deformation parameters are small (as shown on Table I).

Figure 9(b) is the same as Fig. 9(a) except that it is for the deformation reduction factor F. Its value ranges from about 1.0 for oblate daughter nuclei to about 4.3 for ^{238}U with deformation parameters $\beta_2 = 0.215$ and $\beta_4 = 0.102$ and it has small Q value ($Q = 4.3$ MeV). Figure 9(c) shows the combined effect of finite-range *NN* force and the deformation on the value of S_α, it displays the neutron number variation of the ratio of S_α calculated assuming spherical nucleus and zero-range *NN* force and S_α for deformed nucleus derived from finite-range *NN* force. This effect can reduce the value of S_α by an order of magnitude.

IV. CONCLUSION

A study of the effect of the nuclear deformation of the daughter nuclei on the behavior of the α-particle preformation probability S_α is presented. The main effect of antisymmetrization under exchange of nucleons between the α and the deformed daughter nuclei has been included in the folding model through the finite-range exchange part of the *NN* interaction. The variation of S_α with the neutron number for the isotopes of Th, U, Pu, Cm, and Fm is studied.

The study clarifies that the deformation of the daughter nucleus and the finite-range *NN* force can reduce the value of the preformation factor by about an order of magnitude. The reduction for a certain nucleus depends on the Q value and the values and orders of deformation parameters. This leads to change in the behavior of S_α with N or Z numbers when deformation is switched on.

[1] S. Hofmann and G. Munzenberg, Rev. Mod. Phys. **72**, 733 (2000).
[2] P. E. Hodgeson and E. Betak, Phys. Rep. **374**, 1 (2003).
[3] G. Audi, O. Bersillon, J. Blachot, and A. H. Wapstra, Nucl. Phys. A **729**, 3 (2003).
[4] M. Ismail, A. Y. Ellithi, M. M. Botros, and A. Adel, Phys. Rev. C **81**, 024602 (2010).
[5] M. Ismail and A. Adel, Phys. Rev. C **86**, 014616 (2012).
[6] Yibin Qian and Zhongzhou Ren, Phys. Rev. C **88**, 044329 (2013).
[7] Dongdong Ni, Zhongzhou Ren, Tiekuang Dong, and Yibin Qian, Phys. Rev. C **87**, 024310 (2013).
[8] M. Ismail and A. Adel, Phys. Rev. C **88**, 054604 (2013).
[9] Yu. Ts. Oganessian *et al.*, Phys. Rev. C **74**, 044602 (2006).
[10] Yu. Ts. Oganessian, F. Sh. Abdullin, P. D. Bailey, D. E. Benker, M. E. Bennett, S. N. Dmitriev, J. G. Ezold, J. H. Hamilton, R. A. Henderson, M. G. Itkis *et al.*, Phys. Rev. Lett. **104**, 142502 (2010).
[11] Yu. Ts. Oganessian, F. Sh. Abdullin, C. Alexander, J. Binder, R. A. Boll, S. N. Dmitriev, J. Ezold, K. Felker, J. M. Gostic, R. K. Grzywacz *et al.*, Phys. Rev. C **87**, 054621 (2013).
[12] H. Geiger and J. M. Nutall, Phil. Mag. **22**, 613 (1911).
[13] V. E. Viola and G. T. Seaborg, J. Inorg. Nucl. Chem. **28**, 741 (1966).
[14] A. Parkhomenko and A. Sobiczewski, Acta Phys. Pol. B **36**, 3095 (2005).
[15] V. Yu. Denisov and A. A. Khudenko, Phys. Rev. C **79**, 054614 (2009).
[16] C. Xu and Z. Ren, Nucl. Phys. A **753**, 174 (2005).
[17] G. Royer, J. Phys. G: Nucl. Part. Phys. **26**, 1149 (2000).
[18] K. P. Santhosh, Jayesh George Joseph, and Sabina Sahadevan, Phys. Rev. C **82**, 064605 (2010).
[19] K. P. Santhosh and B. Priyanka, Phys. Rev. C **87**, 064611 (2013).
[20] D. N. Basu, Phys. Lett. B **566**, 90 (2003).
[21] P. Roy Chowdhury, C. Samanta, and D. N. Basu, At. Data Nucl. Data Tables **94**, 781 (2008).
[22] M. Ismail, A. Y. Ellithi, M. M. Botros, and A. Abdurrahman, Phys. Rev. C **86**, 044317 (2012).
[23] John O. Rasmussen and Benjamin Segall, Phys. Rev. **103**, 1298 (1956).
[24] K. P. Santhosh and S. Sahadevan, Nucl. Phys. A **847**, 42 (2010).
[25] K. P. Santhosh, J. G. Joseph, and B. Priyanka, Nucl. Phys. A **877**, 1 (2012).
[26] Chang Xu and Zhongzhou Ren, Phys. Rev. C **74**, 014304 (2006).
[27] A. Coban, O. Bayrak, A. Soylu, and I. Boztosun, Phys. Rev. C **85**, 044324 (2012).
[28] V. Yu. Denisov and A. A. Khudenko, At. Data Nucl. Data Tables **95**, 815 (2009).
[29] V. Yu. Denisov and A. A. Khudenko, Phys. Rev. C **81**, 034613 (2010).
[30] M. Ismail and A. Adel, Nucl. Phys. A **912**, 18 (2013).
[31] M. Ismail, M. M. Osman, and F. Salah, Phys. Rev. C **60**, 037603 (1999).
[32] Dao T. Khoa, Phys. Rev. C **63**, 034007 (2001).
[33] G. R. Satchler and W. G. Love, Phys. Rep. **55**, 183 (1979).
[34] M. Ismail and W. M. Seif, Phys. Rev. C **81**, 034607 (2010).
[35] M. Ismail, W. M. Seif, A. Y. Ellithi, and F. Salah, J. Phys. G: Nucl. Part. Phys. **35**, 075101 (2008).
[36] P. Moller, J. R. Nix, W. D. Myers, and W. J. Swiatecki, At. Data Nucl. Data Tables **59**, 185 (1995).
[37] X. Campi and A. Bouyssy, Phys. Lett. B **73**, 263 (1978).
[38] Dao T. Khoa, G. R. Satchler, and W. von Oertzen, Phys. Rev. C **56**, 954 (1997).
[39] B. Buck, A. C. Merchant, and S. M. Perez, Phys. Rev. C **45**, 2247 (1992).
[40] N. G. Kelkar and H. M. Castaneda, Phys. Rev. C **76**, 064605 (2007).
[41] A. Soylu, Y. Sert, O. Bayrak, and I. Boztosun, Eur. Phys. J. A **48**, 128 (2012).
[42] C. Xu and Z. Ren, Phys. Rev. C **73**, 041301(R) (2006).
[43] Madhubrata Bhattacharya, Subinit Roy, and G. Gangopadhyaya, Phys. Lett. B **665**, 182 (2008).
[44] P. Moller, R. Bengtsson, B. G. Carlsson, P. Olivius, T. Ichikawa, H. Sagawa, and A. Iwamoto, At. Data Nucl. Data Tables **94**, 758 (2008).
[45] NUDAT2.6, Nuclear Structure and Decay Data, available from http://www.nndc.bnl.gov/nudat2/